Cell Calcium 101 (2022) 102505

Contents lists available at ScienceDirect

Cell Calcium

journal homepage: www.elsevier.com/locate/ceca

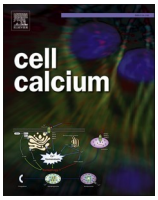

ZnT1 is a neuronal Zn^{2+}/Ca^{2+} exchanger

Noa Gottesman[a], Hila Asraf [a], Milos Bogdanovic [a], Israel Sekler [a], Thanos Tzounopoulos[b], Elias Aizenman [a,c], Michal Hershfinkel [a,*]

[a] Department of Physiology and Cell Biology, and the Zlotowski Center for Neuroscience, Ben-Gurion University of the Negev, Faculty of Health Sciences, POB 653, Beer-Sheva 84108, Israel
[b] Department of Otolaryngology and Pittsburgh Hearing Research Center, University of Pittsburgh School of Medicine, Pittsburgh, PA 15261, United States
[c] Department of Neurobiology and Pittsburgh Institute for Neurodegenerative Diseases, University of Pittsburgh School of Medicine, Pittsburgh, PA 15261, United States

ARTICLE INFO

Keywords:
Zinc transport
ZnT1
Neurotoxicity
Calcium
Zn^{2+}/Ca^{2+} exchange
DIV- days in vitro
WB- western blot
RFP- red fluorescent protein

ABSTRACT

Zinc transporter 1 (ZnT1; SLC30A1) is present in the neuronal plasma membrane, critically modulating NMDA receptor function and Zn^{2+} neurotoxicity. The mechanism mediating Zn^{2+} transport by ZnT1, however, has remained elusive. Here, we investigated ZnT1-dependent Zn^{2+} transport by measuring intracellular changes of this ion using the fluorescent indicator FluoZin-3. In primary mouse cortical neurons, which express ZnT1, transient addition of extracellular Zn^{2+} triggered a rise in cytosolic Zn^{2+}, followed by its removal. Knockdown of ZnT1 by adeno associated viral (AAV)-short hairpin RNA (shZnT1) markedly increased rates of Zn^{2+} rise, and decreased rates of its removal, suggesting that ZnT1 is a primary route for Zn^{2+} efflux in neurons. Although Zn^{2+} transport by other members of the SLC30A family is dependent on pH gradients across cellular membranes, altered H^+ gradients were not coupled to ZnT1-dependent transport. Removal of cytoplasmic Zn^{2+}, against a large inward gradient during the initial loading phase, suggests that Zn^{2+} efflux requires a large driving force. We therefore asked if Ca^{2+} gradients across the membrane can facilitate Zn^{2+} efflux. Elimination of extracellular Ca^{2+} abolished Zn^{2+} efflux, while increased extracellular Ca^{2+} levels enhanced Zn^{2+} efflux. Intracellular Ca^{2+} rises, measured in GCaMP6 expressing neurons, closely paralleled cytoplasmic Zn^{2+} removal. Taken together, these results strongly suggest that ZnT1 functions as a Zn^{2+}/Ca^{2+} exchanger, thereby regulating the transport of two ions of fundamental importance in neuronal signaling.

Introduction

Although zinc is critical for neuronal development, survival and function [1, 2], cytoplasmic accumulation of excess zinc ions (Zn^{2+}) can be neurotoxic [1, 3]. As such, tight regulation of intracellular Zn^{2+} concentrations by its compartmentalization is essential for proper neuronal function [2]. Numerous Zn^{2+} transporters from both the ZnT (SLC30A) and ZIP (SLC39A) families of proteins are present in neurons, and they function to transfer the metal ion either from (ZnTs) or into (ZIPs) the cytoplasm [4–6]. One of the best characterized neuronal transporters is ZnT3 (SLC30A3), which is essential for accumulation of Zn^{2+} in synaptic vesicles in a large number of excitatory and inhibitory synapses throughout the brain [7–11]. Synaptic Zn^{2+} is released during neuronal activity and plays an important role in shaping neuronal signaling and synaptic responses [9, 12–15], notably by modulating the activity of postsynaptic NMDA receptors [10, 16, 17]. In addition to ZnT3, ZnT1 (SLC30A1) is also necessary for Zn^{2+} regulation of the Zn^{2+}-sensitive GluN2A-containing NMDA receptors [17]. ZnT1 is a highly conserved and ubiquitously expressed protein [18, 19] present on the plasma membrane of both neurons and glia [20–23]. Silencing of ZnT1 expression in cultured cells can strongly modulate Zn^{2+} toxicity, and global knockout of this transporter is embryonically lethal [21, 24]. Expression levels and activity of ZnT1 are highly regulated by changes in cytoplasmic Zn^{2+} [25–27], suggesting that this transporter plays an important role in Zn^{2+} homeostasis. In neurons, ZnT1 has reduces cytosolic Zn^{2+} accumulation following prolonged (30 min) incubation with the metal ion [24]. ZnT1 is enriched at the postsynaptic density, and by limiting postsynaptic Zn^{2+} accumulation following its translocation from presynaptic release sites [22, 23, 28], it protects neurons from Zn^{2+} toxicity.

Despite the well-established function of ZnT1 on neuromodulation and neuroprotection, the mechanism of ZnT1 transport remains

; ZnT1-, Zn^{2+} transporter 1; DIV-, days in vitro; RFP-, red fluorescent protein; WB-, western blot.

* Corresponding author.
E-mail address: hmichal@bgu.ac.il (M. Hershfinkel).

https://doi.org/10.1016/j.ceca.2021.102505
Received 18 July 2021; Received in revised form 31 October 2021; Accepted 22 November 2021
Available online 23 November 2021

unknown. ZnT family members expressed in acidic intracellular organelles function as Zn^{2+}/H^{+} exchangers [29, 30], primarily as a result of the strong pH-dependence of a highly conserved, histidine-rich Zn^{2+} binding site on the protein [31, 32]. However, this mechanism may not account for ZnT1-mediated Zn^{2+} transport, as proton gradients across the neuronal plasma membrane may be negligible under normal physiological conditions [33, 34]. This suggests a different mechanism is required to facilitate ZnT1-dependent Zn^{2+} transport which is, indeed, described in the present study.

Results

ZnT1 functions to extrude Zn^{2+} in cortical neurons

We first carried out immunostaining for ZnT1, together with either the axonal marker Tau or the dendritic marker MAP2, and observed abundant presence of the transporter throughout the somata as well as processes in cultured mouse cortical neurons (Fig. 1A,B, Mander's coefficient of 0.7 ± 0.1 for Tau and 0.7 ± 0.2 for MAP2, $n = 4$). In agreement with previous studies [17, 35], we also found that ZnT1 is tightly co-localized with the GluN2A subunit of the NMDA receptor in these cells (Fig. 1C, Mander's coefficient of 0.9 ± 0.1, $n = 5$). Next, in order to reduce ZnT1 expression levels in neurons, we assembled an AAV2 hSyn virus encoding a sequence aimed to silence ZnT1 (shZnT1) carrying an RFP fluorescent tag to detect positively infected cells. Infection rates were high, as approximately 80–90% of neurons in the cultures were positive for RFP. Effective silencing of the transporter was confirmed by qPCR analysis of ZnT1 mRNA levels (Fig. 1D), as well as by immunoblot analysis of protein expression levels (Fig. 1E and Supplemental Fig. 1A). Both analyses demonstrated approximately 50% knockdown of ZnT1. Consistent with mRNA downregulation, cortical cultures infected with shZnT1 showed similar 50% decrease in ZnT1 immunofluorescence, when compared to ZnT1 levels from control cultures infected with an RFP-expressing virus only (Fig. 1F). Importantly, neurons infected with shZnT1 did not exhibit significant alteration in mRNA expression of other neuronal ZnTs or ZIPs (Supplemental Fig. 1B). These results indicate that viral expression of shZnT1 selectively reduces ZnT1 expression.

Next, we evaluated whether silencing ZnT1 would result in decreased Zn^{2+} efflux following a short exposure to Zn^{2+}. Cortical

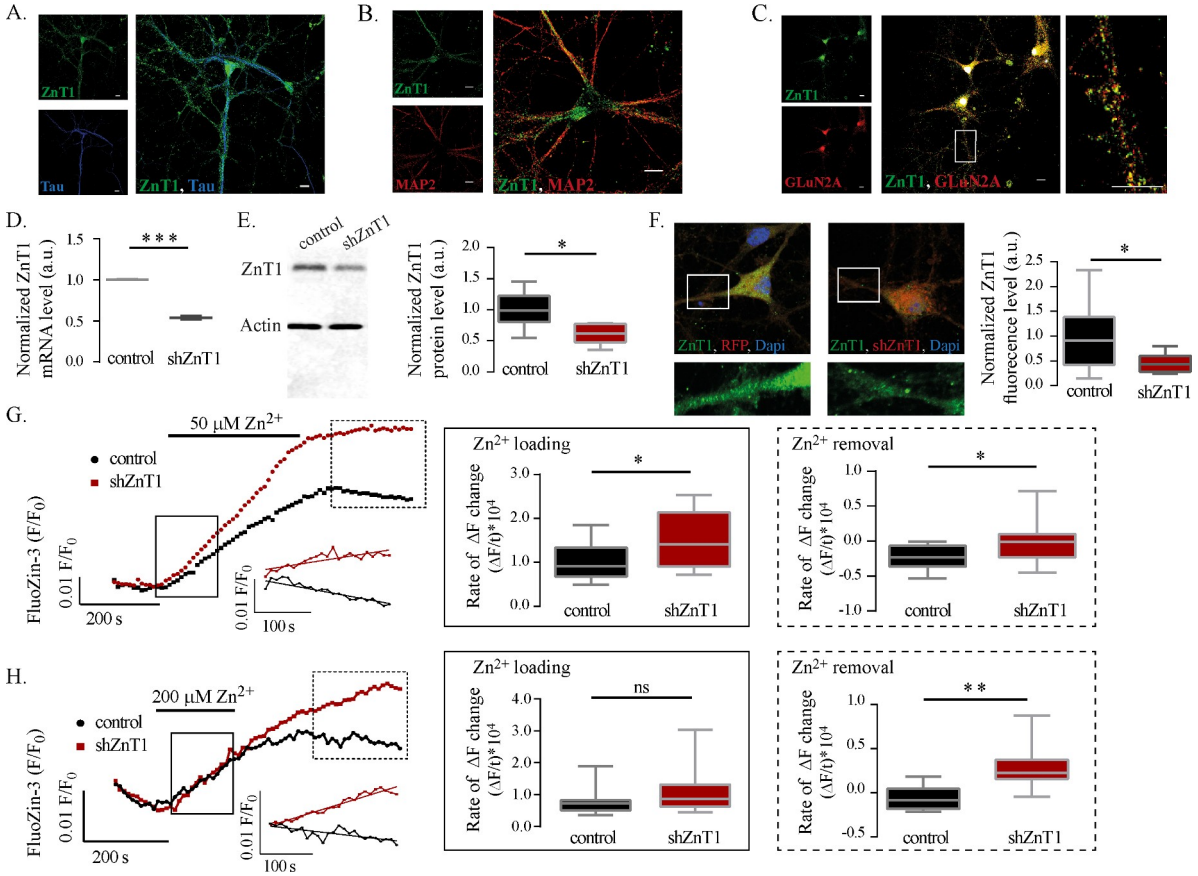

Fig. 1. ZnT1 is required to extrude Zn^{2+} in cortical neurons. (A) Representative images of ZnT1 immuno-staining (green) in mouse cortical cultures with anti-Tau (blue) axonal marker (X60), with (B) anti-MAP2 (red) dendritic marker (X60), or with (C) anti-GluN2A subunit of NMDAR (X20). Scale bar is 10 µM. (D) ZnT1 mRNA levels after AAV2 hSyn shZnT1 or control infection of cortical neurons. ($n = 3$, *t*-test, ***$p = 0.007$) (E) WB analysis of neurons virally infected as in D, right panel shows densitometry analysis of protein levels normalized to actin ($n = 5$, *t*-test, *$p = 0.02$). (F) Representative image of immuno-fluorescent labeling of shZnT1 (X60) and control infected neurons with anti-ZnT1 (green), RFP fluorescence of the virus (red), and DAPI (blue). Lower panel shows ZnT1 staining along a process, zoom over the area marked by the box. Right panel is quantification of ZnT1 staining level along isolated processes ($n = 12$, *t*-test, *$p = 0.01$,). (G) Cortical neurons, infected with shZnT1 or control virus as in D, were loaded with the Zn^{2+} sensitive, cell permeant, FluoZin-3 and treated with 50 µM Zn^{2+} as indicated, and then washed with Zn^{2+}-free solution. Representative traces of the fluorescent signal are shown. Insert shows magnification of aligned traces during Zn^{2+} removal phase (dashed box). Middle panel shows averaged initial rates of fluorescence increase (marked by box, Zn^{2+} loading), calculated over the first 100 s following addition of Zn^{2+}. ($n = 13$, *t*-test, *$p = 0.02$). Right panel shows averaged rate of fluorescence change upon wash with Zn^{2+}-free solution (marked by dashed box, Zn^{2+} removal), calculated over 200 s, from the maximal signal. ($n = 13$, *t*-test, *$p = 0.04$). (H) Virally infected neurons, as in G, were treated with 200 µM Zn^{2+} and representative traces of FluoZin-3 are shown, with the insert showing the aligned traces during the Zn^{2+} removal phase. Middle and right panels show rates of fluorescence change during the loading (marked by box) and removal (marked by dashed box) phases. ($n = 13$, *t*-test, ns-non significant, with $p = 0.22$ and, **$p = 0.002$ respectively) For interpretation of the references to color in this figure legend, the reader is referred to the web version of this article.).

cultures were loaded with the cell permeant form of the Zn^{2+}-selective fluorescent indicator FluoZin-3 [36] and then transiently exposed to 50 μM Zn^{2+}, yielding an increase in fluorescence. Changes in FluoZin-3 fluorescence represent the net cytosolic rise of Zn^{2+} concentration, resulting from the combined influx of the ion into the cell and its concomitant removal from the cytoplasm. The transient Zn^{2+} exposure was then followed by treatment with a Zn^{2+}-free extracellular solution. Changes in FluoZin-3 fluorescence at this stage represent primarily the efflux of Zn^{2+} from the cytoplasmic compartment. We observed that during the initial Zn^{2+} exposure, the rate of Zn^{2+} rise was significantly faster in ZnT1 knockdown (shZnT1) neurons compared to control, ZnT1-expressing cells (Fig. 1G). This suggests that during transient exposure to extracellular Zn^{2+}, ZnT1-dependent Zn^{2+} efflux strongly counteracts the inward movement of the ion. Upon removal of Zn^{2+} from the extracellular solution, the decrease in cytosolic Zn^{2+} (negative rate) was faster in control cells when compared to shZnT1 cells (Fig. 1G, right panel). Thus, Zn^{2+} efflux is much slower in ZnT1-defficient neurons. The Zn^{2+} removal rate, however, may be influenced by the overall level of accumulated Zn^{2+}, as well as FluoZin-3 occupancy [37], which was notably higher in shZnT1 cells (red trace) when compared to controls. To correct for this potential confound, we utilized a higher Zn^{2+} concentration (200 μM) during the initial exposure. At this high concentration of Zn^{2+}, we expect that transport activity mediated by ZnT1 would not be able to effectively counteract rapid influx of Zn^{2+}. Indeed, note that the rates of FluoZin-3 fluorescence increase under these conditions were not significantly different between shZnT1 and control cells, leading to similar Zn^{2+} accumulation (Fig. 1H). Upon Zn^{2+} removal from the extracellular solution, we again observed a more pronounced decrease in fluorescence (i.e. Zn^{2+} efflux) in control cells when compared to shZnT1 cells (Fig. 1H). These results strongly suggest that decreased expression of ZnT1 impairs Zn^{2+} efflux in cortical neurons, indicating that ZnT1 is the predominant Zn^{2+}-extruder in neurons.

If ZnT1 is a major route for Zn^{2+} extrusion in neurons, then enhanced Zn^{2+} efflux rates would be expected in cells with increased ZnT1 expression. Cortical neurons were thus pre-exposed to Zn^{2+} (50 μM in MEM containing 0.01% BSA for 12 h), a condition that enhances ZnT1 expression via activation of the metal response element transcription factor 1 (MTF-1) [26]. Indeed, mRNA analysis confirmed a nearly 4-fold enhancement in neuronal ZnT1 expression under these conditions, when compared to vehicle-treated (control) cells (Fig. 2A). Immunoblot and immuno-fluorescence analysis of ZnT1 protein levels showed a less pronounced, albeit significant, effect of approximately two-fold increase of ZnT1 expression in Zn^{2+} pre-treated cells (Fig. 2B,C). Importantly, this Zn^{2+} treatment was not neurotoxic, as evidenced by similarly low levels lactate dehydrogenase (LDH) activity, an index of cellular damage [38], in the extracellular fluid obtained from control and Zn^{2+} pre-treated cultures (Fig. 2D). Although mRNA expression of other plasma membrane ZnTs and ZIPs did not change significantly by this

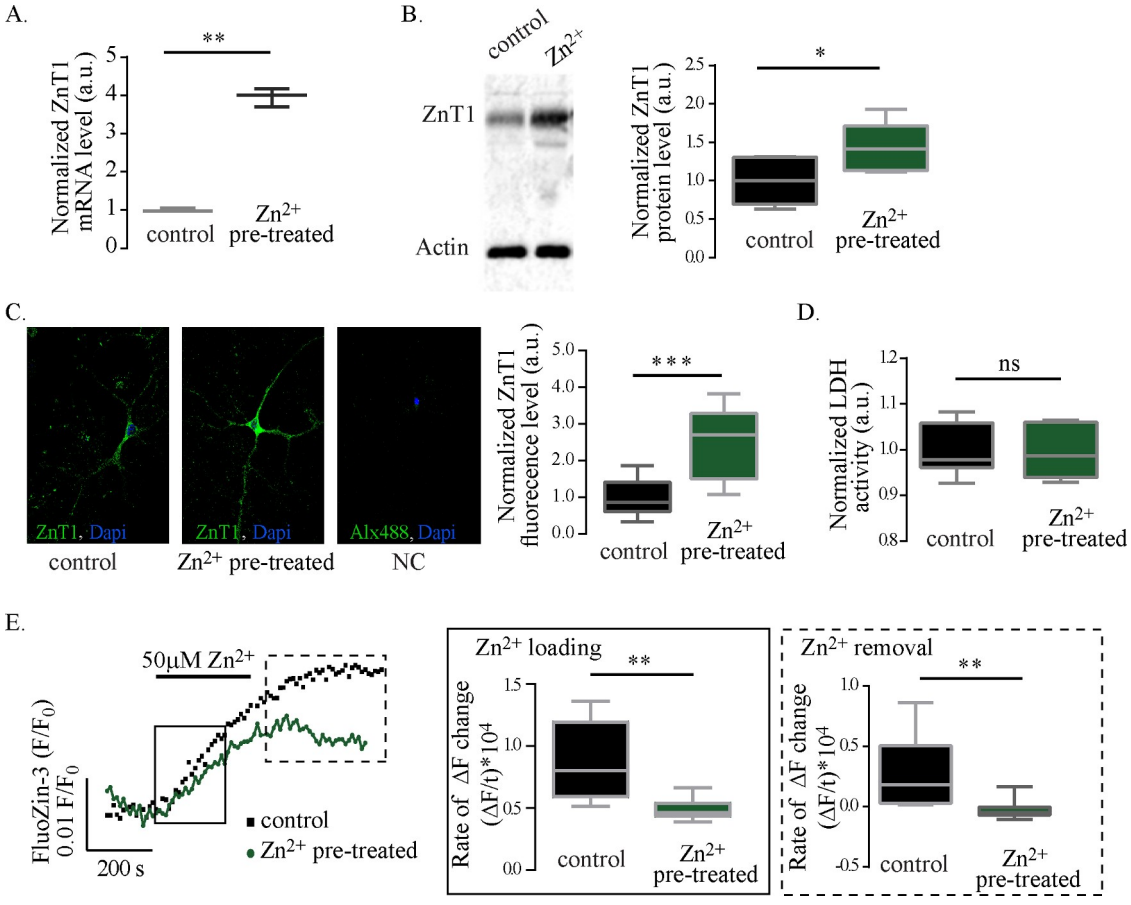

Fig. 2. Elevated ZnT1 levels in cortical neurons enhance Zn^{2+} efflux. Cortical cultured mouse neurons were pre-treated with 50 μM Zn^{2+} in the presence of 0.01% BSA for 12 h to enhance ZnT1 expression, or control cells not treated with Zn^{2+}. (A) ZnT1 mRNA levels ($n = 3$, *t*-test, $^{**}p = 0.001$) and (B) protein levels measured with WB and quantified using densitometry. ($n = 6$, *t*-test, $^{*}p = 0.02$). (C) Representative immunofluorescence images of ZnT1 expression using anti-ZnT1 antibodies (left panels, NC- negative control without primary antibody) and its quantification (right panel, $n = 4$, *t*-test, $^{***}p = 0.0001$). (D) LDH activity in neurons treated with Zn^{2+} as described compare to control ($n = 3$, *t*-test, ns-non-significant). (E) Representative traces of FluoZin-3 fluorescence in cortical neurons pre-treated with Zn^{2+} or controls, that are transiently perfused with 50 μM Zn^{2+} as indicated. Middle and right panels show initial rates of fluorescence change during the loading (marked by box, rate during initial 100 s following addition of Zn^{2+}) and removal (marked by dashed box, rate during 200 s period following the maximal signal) phases. ($n = 14$, *t*-test, $^{**}p = 0.003$).

treatment, we did observe a very slight but significant decrease of the vesicular Zn^{2+} transporter ZnT3 as a result of the Zn^{2+} pre-treatment (Supplemental Fig. 1C). Next, we monitored Zn^{2+} transport using FluoZin-3. Neurons were incubated with a cell permeant Zn^{2+} chelator (0.5 μM TPEN, 15 min. following FluoZin-3 loading) to reduce baseline fluorescence that remained relatively high following Zn^{2+} pre-treatment, and subsequently extensively washed with a Zn^{2+}-free solution to remove excess TPEN. We then monitored changes in FluoZin-3 fluorescence in neurons transiently exposed to 50 μM Zn^{2+} as described earlier. Neurons pre-treated with Zn^{2+}, and thus with increased ZnT1 expression level, demonstrated significantly slower rates of Zn^{2+} rise that yielded overall decreased maximal fluorescent signal, when compared to control neurons (Fig. 2E). In addition, upon extracellular Zn^{2+} removal, neurons pre-treated with Zn^{2+} exhibited a more pronounced cytoplasmic Zn^{2+} efflux. Since ZnT3 acts to remove cytosolic Zn^{2+} by accumulating it in synaptic vesicles, it is noted that the slightly lower expression may account for a small increase in cytosolic Zn^{2+} accumulation, leading to an underestimation of the rate of ZnT1-dependent efflux. Altogether, these results indicate that ZnT1 expression levels regulate intracellular neuronal Zn^{2+} concentrations by influencing the extrusion rates of the ion.

pH changes affect cytoplasmic Zn^{2+} levels in neurons but do not drive Zn^{2+} removal

Members of the ZnT family expressed in organelles with an acidic lumen act as Zn^{2+}/H^+ exchangers to transport cytoplasmic Zn^{2+} into the organelles [30]. Indeed, disruption of vesicular proton gradients strongly attenuates Zn^{2+} transport via ZnT5 and ZnT2 [29, 39]. If ZnT1 were also a Zn^{2+}/H^+ exchanger, then we would expect that acidic extracellular pH would enhance ZnT1-dependent Zn^{2+} efflux. To test for this, neurons loaded with FluoZin-3 were initially exposed to 200 μM Zn^{2+} at pH 7.4, to allow its rapid cytoplasmic accumulation. We then monitored rates of Zn^{2+} efflux in neurons perfused with Zn^{2+}-free extracellular solutions at pH 6. This pH enhances the H^+ inward gradient and would therefore be expected to enhance Zn^{2+} efflux, manifested as a faster decrease in FluoZin-3 signal upon removal of extracellular Zn^{2+}. Yet, we observed that FluoZin-3 fluorescence continued to dramatically increase during the Zn^{2+}-free, pH 6 treatment (Fig. 3A). Since Zn^{2+} is not present in the extracellular solution during this stage, the increased levels of intracellular Zn^{2+} are likely generated from other sources. Nonetheless, the more pronounced H^+ gradient is not sufficient to enhance Zn^{2+} efflux, which would be expected to reduce its rate of accumulation. Moreover, if ZnT1 were a Zn^{2+}/H^+ exchanger, perfusion of the cells with an alkaline solution (pH 8) would decrease or prevent Zn^{2+} removal by increasing the outward H^+ gradient. Following the cytosolic Zn^{2+} rise (200 μM Zn^{2+} at pH 7.4), we observed that Zn^{2+} removal rates in neurons exposed to a pH 8, Zn^{2+}-free, solution were not different than rates in cells exposed to physiological pH levels (Fig. 3A). These results strongly suggest that, unlike vesicular ZnT transporters, ZnT1 does not likely function as a Zn^{2+}/H^+ exchanger in cortical neuronal plasma membranes.

We then asked whether this paradigm triggers changes in intracellular pH using cells loaded with the fluorescent pH-sensitive indicator BCECF. Neurons were transiently exposed to 200 μM Zn^{2+} (pH 7.4), which we previously showed led to rapid cytosolic Zn^{2+} accumulation (Fig. 3A). This Zn^{2+} influx produced no changes in intracellular pH (Fig. 3B). It is conceivable that even if H^+/Zn^{2+} exchange had occurred, it may have not been sufficient to affect cytosolic pH. Subsequent extracellular Zn^{2+} removal and perfusion with acidic (pH 6) solution led to pronounced intracellular acidification (Fig. 3B). Note that this cytoplasmic acidification was concurrent with the previously noted intracellular Zn^{2+} accumulation (Fig. 3C). Prior studies showed liberation of Zn^{2+} from intracellular sources by similar brief cytoplasmic acidification [40]. Thus, liberation of Zn^{2+} is likely responsible for the enhanced accumulation we observed during exposure of the cells to acidic, Zn^{2+}-free, solution (Fig. 3A). It may be argued that the Na^+/H^+ exchanger [41, 42] may mask ZnT1-dependent H^+ transport. However, our results show that the small pH changes observed are not followed by a recovery of pH, which is a hallmark of Na^+/H^+ exchanger [41, 42]. As such, these results show that ZnT1-dependent Zn^{2+} efflux is not coupled to H^+ influx.

Finally, we asked whether ZnT1-dependent Zn^{2+} efflux could still modulate the rate of Zn^{2+} rise, triggered by its liberation during acidification. To test this, we compared rates of Zn^{2+} removal in control and shZnT1 neurons. Transient exposure to 200 μM extracellular Zn^{2+} (pH 7.4) resulted in comparable rates of cytoplasmic Zn^{2+} rise in both control and shZnT1-expressing neurons (Fig. 3D), as described earlier (Fig. 1H). Neurons were then washed with a Zn^{2+}-free acidic (pH 6) solution. We observed similar increases in FluoZin-3 fluorescence in control and shZnT1 neurons, suggesting that pH-dependent cytoplasmic Zn^{2+} accumulation, following removal of extracellular Zn^{2+}, was independent of ZnT1 expression (Fig. 3D,E). Notably, these large increases in cytoplasmic Zn^{2+} were not observed in shZnT1 neurons when, as described earlier, the Zn^{2+}-free treatment was performed at neutral pH. These results indicate that acidic pH-dependent Zn^{2+} accumulation is not influenced by ZnT1 and is largely due to the intracellular liberation of Zn^{2+} [40]. It must be noted that neuronal H^+-dependent Zn^{2+} transport had been previously observed [43, 44] and closely linked to the activity of ZIP transporters [44]. Our results clearly indicate that knockdown of ZnT1 does not affect the pH dependent intracellular Zn^{2+} rise, therefore we conclude that ZnT1 is not a component of the previously described Zn^{2+}/H^+ exchange.

ZnT1 is a neuronal Zn^{2+}/Ca^{2+} exchanger

The results described thus far do not support the possibility that ZnT1 couples Zn^{2+} efflux to H^+ transport, and therefore it requires a different counter-ion. Considering that ZnT1-dependent Zn^{2+} efflux can act against an inward gradient and modulate the initial rate of cytosolic Zn^{2+} rise (Fig. 1G), suggests that a strong counter driving force is present. We hypothesized that the large Ca^{2+} gradients across the neuronal plasma membrane [45] may provide this driving force. To test this hypothesis, we measured the rates of Zn^{2+} removal in the presence or absence of extracellular Ca^{2+}. We monitored fluorescence changes in FluoZin-3 loaded neurons that were initially exposed to Zn^{2+} (200 μM) at physiological Ca^{2+} concentrations (1.8 mM), and subsequently we determined rates of Zn^{2+} efflux while perfusing with extracellular Zn^{2+}-free solutions containing or devoid of Ca^{2+}. In support of our hypothesis, the cytoplasmic Zn^{2+} removal, manifested as a decrease in FluoZin-3 fluorescence (negative rate), was observed only when Ca^{2+} was present in the wash solution (Fig. 4A). When we varied the Ca^{2+} concentration during the Zn^{2+} removal phase, we noted that higher levels of Ca^{2+} (5 mM) accelerated the rates of Zn^{2+} transport (Fig. 4A). These results strongly argue that extracellular Ca^{2+} is critical for Zn^{2+} efflux. As rapid Zn^{2+} influx can be mediated through Ca^{2+} channels [46], particularly L-Type Ca^{2+} Channels (LTCC) [47, 48], we monitored Zn^{2+} transport in the presence of an LTCC inhibitor, nifedipine (1 μM). Rates of Zn^{2+} rise following exposure to 200 μM Zn^{2+} were not inhibited by nifedipine (Fig. 4B), likely because synchronous voltage changes sufficient to open LTCC are not induced in our experiment. Furthermore, Zn^{2+} removal rates were also not affected by nifedipine, suggesting that LTCC likely do not play a role in Zn^{2+} efflux. Next, we investigated whether the absence of extracellular Ca^{2+} would influence rates of Zn^{2+} rise during the Zn^{2+} exposure phase. Indeed, we observed intracellular Zn^{2+} rises at rates that were nearly 2-fold higher in the absence of extracellular Ca^{2+} (Fig. 4C). This pronounced change in Zn^{2+} rises was, in fact, highly reminiscent of the Zn^{2+} rises observed in shZnT1 cells (Fig. 1G), suggesting that the presence of extracellular Ca^{2+} is essential for the ZnT1-dependent Zn^{2+} efflux that occurs while neurons are exposed to extracellular Zn^{2+}. Importantly, upon removal of extracellular Zn^{2+}, the Zn^{2+} efflux phase was absent in Ca^{2+}-free solutions

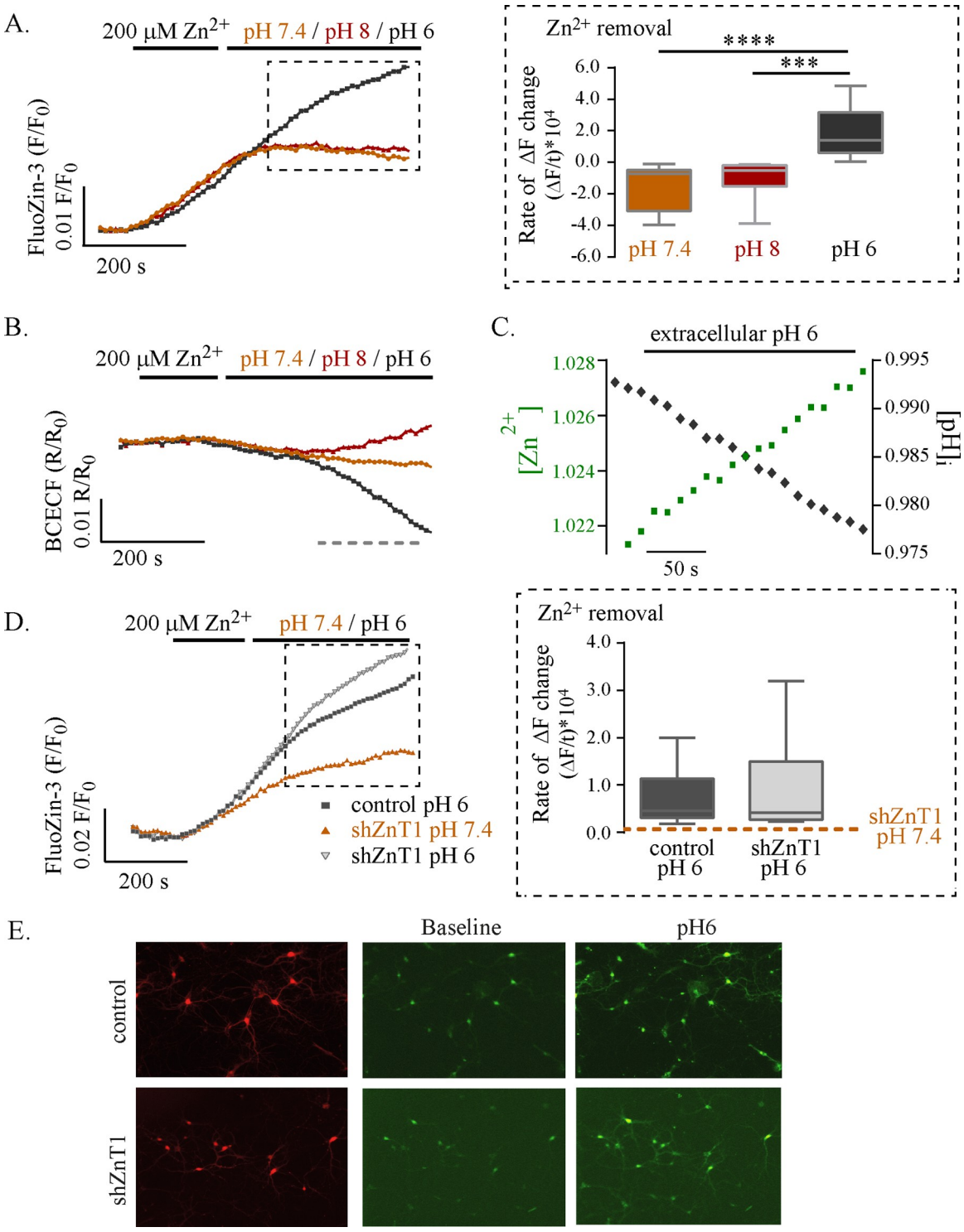

Fig. 3. ZnT1 does not show Zn^{2+}/H^{+} reciprocal activity in cortical neurons. (A) FluoZin-3 fluorescence of cortical neurons, treated with 200 μM Zn^{2+} as indicated. Subsequent wash was done with Zn^{2+}-free solutions at different pH as indicated. Right panel shows averaged rate of Zn^{2+} removal (marked by dashed box, 200 s period following the maximal signal, $n = 12$, ANOVA, ***$p = 0.003$, ****$p < 0.0001$). (B) Traces of fluorescence signals from cortical neurons loaded with the pH sensitive dye BCECF, that were treated transiently with 200 μM Zn^{2+} as in A. (C) Overlap of traces obtained with FluoZin-3 (green) and BCECF (black), taken from A and B, during the Zn^{2+} removal phase (marked by the dashed line in B), showing that cytosolic Zn^{2+} continues to accumulate concomitant with cytosolic pH decrease. (D) Representative traces of FluoZin-3 fluorescence from shZnT1 and control neurons, that were transiently treated with 200 μM Zn^{2+} (pH 7.4) and subsequently perfused with Zn^{2+}-free solution at the indicated pH value. Right panel shows averaged rates of Zn^{2+} removal (marked by dashed box, rate during 200 s period following the maximal signal), dashed red line represents the average rate of Zn^{2+} removal in shZnT1 neurons washed with solution at pH 7.4, as obtained in Fig. 1. ($n = 7$, *t*-test, ns- not significant) (E) Cortical neurons were infected with the AAV2 hSyn shZnT1 or control virus (as in Fig. 1) and loaded with FluoZin-3. Representative images from control and shZnT1 neurons, as in Fig. 3D, showing RFP fluorescence (red, left panels) and FluoZin-3 fluorescence (green), during baseline acquisition (middle panels) and after perfusion with solution at pH 6 (right panels) For interpretation of the references to color in this figure legend, the reader is referred to the web version of this article.).

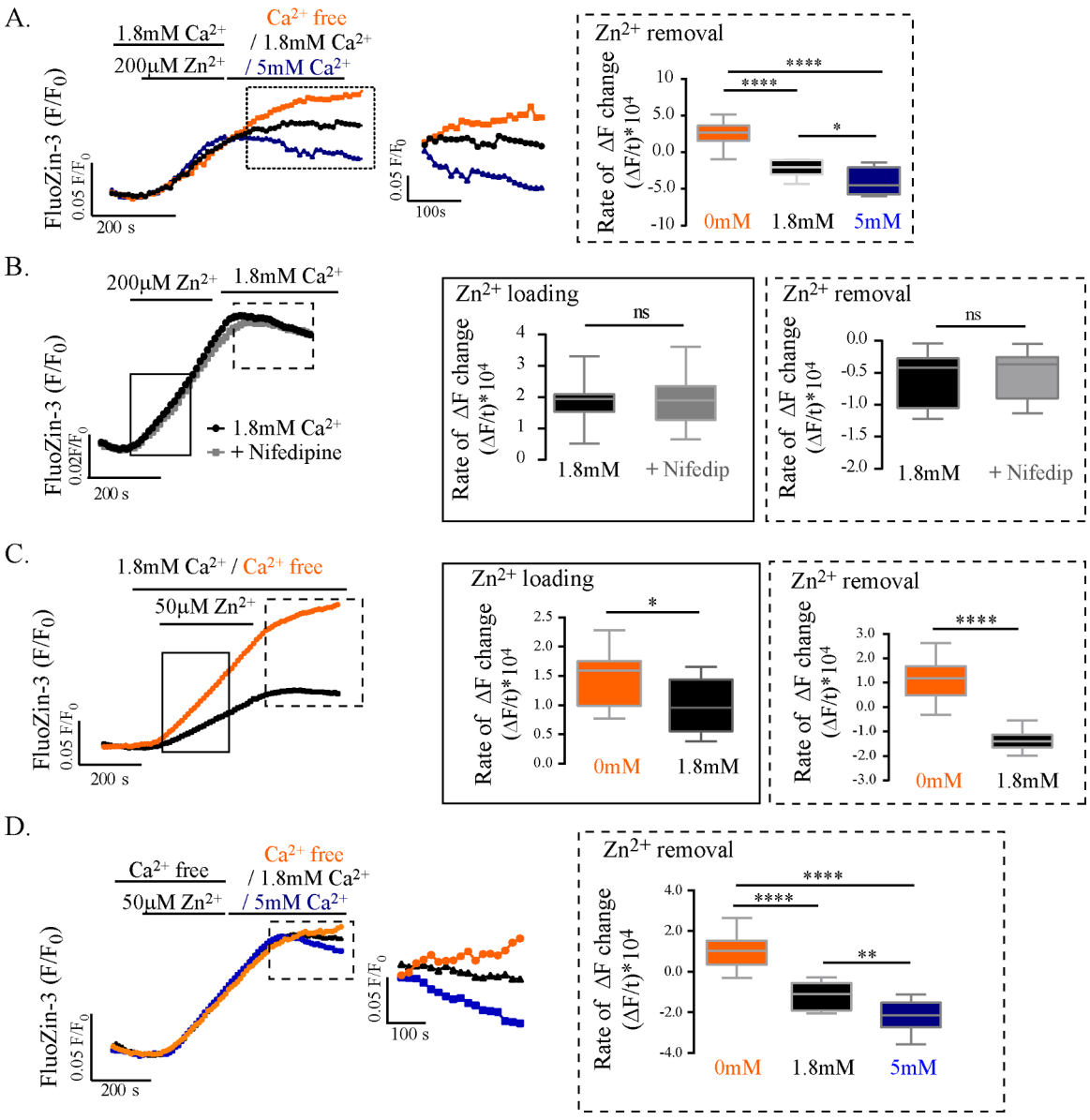

Fig. 4. ZnT1 transport is Ca^{2+}-dependent. (A) Representative traces of FluoZin-3 fluorescence in cultured cortical neurons, transiently treated with 200 μM Zn^{2+} in a solution containing 1.8 mM Ca^{2+}. Neurons were then washed with a solution containing Ca^{2+} at the indicated concentration. Insert shows the Zn^{2+} removal phase (region marked by the dashed box). Right panel shows averaged rate of Zn^{2+} removal (rate during 200 s period following the maximal signal, as marked by the dashed box, $n = 10$, ANOVA, *$p = 0.04$, ****$p < 0.0001$). (B) Representative traces of FluoZin-3 loaded neurons treated with Zn^{2+} as in A (black trace) or in the presence of 1 μM nifedipine (gray trace). Right panel shows averaged rate of Zn^{2+} loading (marked by box, rate during initial 100 s following addition of Zn^{2+}) and Zn^{2+} removal (marked by dashed box, rate during 200 s period following the maximal signal, $n = 14$, *t*-test, ns- not significant). (C) FluoZin-3 fluorescence from neurons perfused with 50 μM Zn^{2+} in a Ca^{2+}-free solution or in a solution containing 1.8 mM Ca^{2+}. Averaged rates of Zn^{2+} loading (marked by box, rate during initial 100 s following addition of Zn^{2+}) and removal (marked by dashed box, rate during 200 s period following the maximal signal) are shown in the middle and right panels. ($n = 10$, *t*-test, *$p = 0.03$, ****$p < 0.0001$) (D) FluoZin-3 fluorescence in cultured cortical neurons transiently treated with 50 μM Zn^{2+} in Ca^{2+}-free solution, followed by perfusion with solution containing Ca^{2+} at the indicated concentrations. Insert shows the Zn^{2+} removal phase (region marked by dashed box). Right panel shows averaged rates of Zn^{2+} removal (rate during 200 s period following the maximal signal, $n = 12$, ANOVA, **$p = 0.003$, ****$p \leq 0.0001$).

(Fig. 4C). Further supporting a link between Zn^{2+} efflux and extracellular Ca^{2+}. Finally, if ZnT1-dependent efflux counteracted Zn^{2+} loading when cortical neurons were exposed to 50 μM Zn^{2+} (Fig. 1G), then we expect that in the absence of extracellular Ca^{2+} this concentration of Zn^{2} would be sufficient to significantly increase cytosolic Zn^{2+}. We therefore determined rates of Zn^{2+} efflux following transient exposure of neurons to only 50 μM Zn^{2+} in Ca^{2+}-free solutions. Upon removal of Zn^{2+}, we monitored a significant decrease in FluoZin-3 fluorescence in the presence of extracellular Ca^{2+} (1.8 mM), but not when cells were washed with Ca^{2+}-free solution (Fig. 4D). Moreover, initial rates of Zn^{2+} removal were enhanced by the presence of 5 mM Ca^{2+} (Fig. 4D). We also noted that rates of Zn^{2+} efflux in this paradigm were comparable to the rates obtained following loading of 200 μM Zn^{2+} in Ca^{2+}-containing solutions (Fig. 4A). These results strongly suggest that extracellular Ca^{2+} is coupled to ZnT-dependent Zn^{2+} efflux in neurons.

While the previous experiments show that the Zn^{2+} efflux properties of ZnT1 are Ca^{2+}-dependent, it remains to be established whether ZnT1 is a Zn^{2+}/Ca^{2+} exchanger. If this were to be the case, Ca^{2+} ions should be transported into neurons concomitantly with Zn^{2+} extrusion. To monitor intracellular Ca^{2+}, we infected cortical neurons with a viral vector encoding the Ca^{2+} fluorescent reporter GCaMP6 [49, 50]. These cells were exposed to 200 μM Zn^{2+} in the presence of physiological Ca^{2+}

concentrations (1.8 mM) in order to trigger Zn^{2+} influx. Under these conditions, we observed no changes in GCaMP6 fluorescence (Figs. 5A, B). However, during the Zn^{2+}-free treatment that followed, we noted pronounced increases in GCaMP6 signals (Fig. 5A,B), suggesting that the Zn^{2+} efflux was accompanied by a measurable Ca^{2+} influx. Control cells that were not treated with Zn^{2+} demonstrated stable intracellular Ca^{2+} levels for the duration of the experiment (Fig. 5A). Regardless of prior treatment, exposure to 10 μM glutamate produced a marked increase in

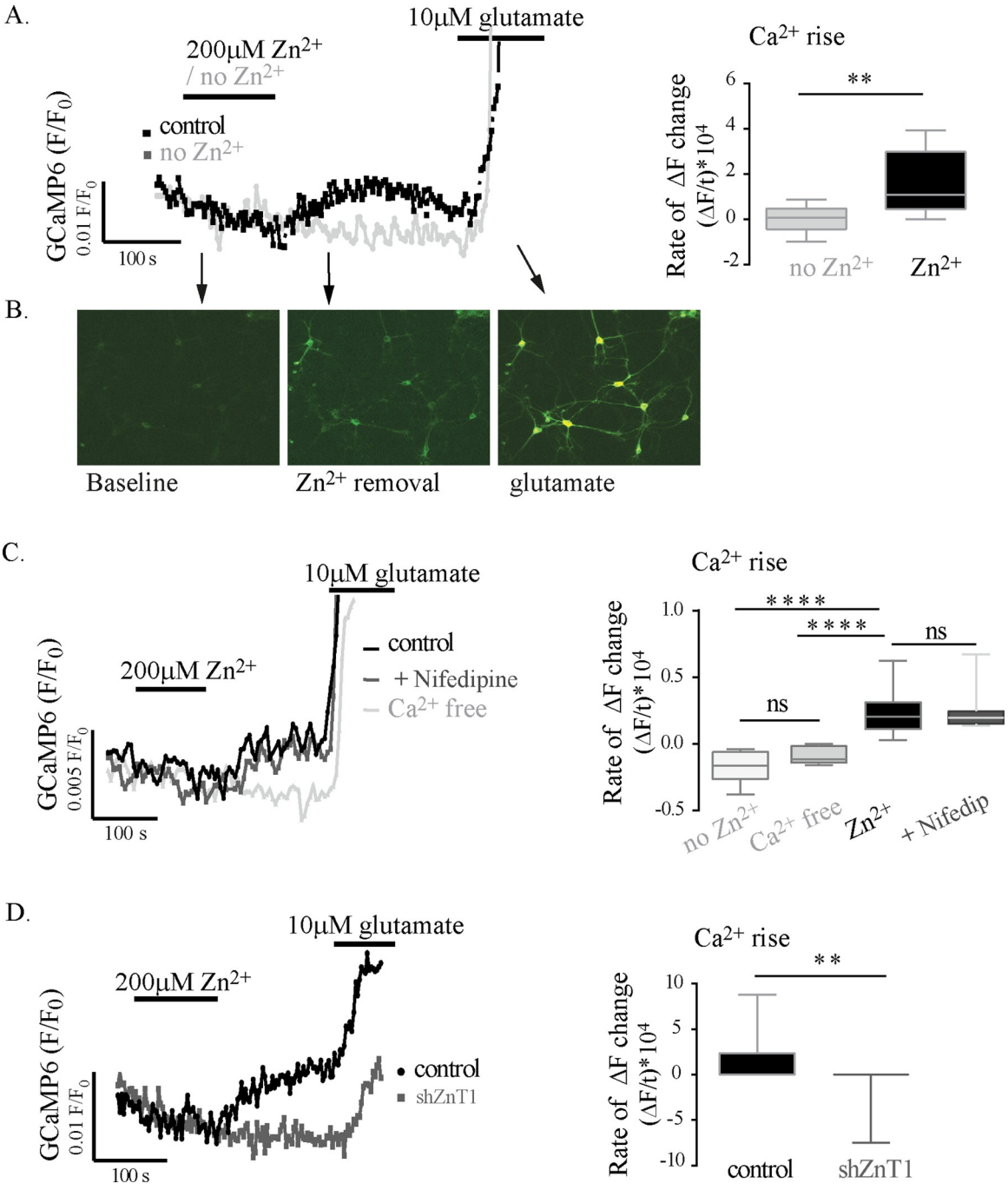

Fig. 5. Reciprocal Ca^{2+} transport in ZnT1 expressing cortical neurons. (A) Representative fluorescent signal from cortical neurons expressing the Ca^{2+} sensitive GCaMP6 indicator. Neurons were perfused with solution containing 1.8 mM Ca^{2+} and were transiently treated with 200 μM Zn^{2+} (black trace) or without Zn^{2+} as control (gray trace). Neurons were then washed with Zn^{2+}-free and Ca^{2+}-containing solution, as in Fig. 4. Finally, glutamate was added to trigger a metabotropic Ca^{2+} response, indicating that physiological cytosolic Ca^{2+} responses are apparent in both cultures. Right panel shows averaged rates of GCaMP6 fluorescence change during the initial 60 s following removal of Zn^{2+} ($n = 10$, t-test, $^{**}p = 0.006$). (B) Representative images of GCaMP6 fluorescence signal obtained at indicated time points, for a Zn^{2+} treated culture as described in A. (C) Representative traces from GCaMP6 expressing cells treated with Zn^{2+} as in A (black trace) or in the presence of 1 μM nifedipine (dark gray trace). In addition, neurons expressing GCaMP6 were treated with Zn^{2+} (as indicated) and then washed with Ca^{2+}-free solution (light gray trace). As control, glutamate was applied, indicating that physiological Ca^{2+} signals are apparent in all cultures. Right panel shows averaged rates of GCaMP6 fluorescence change during the initial 60 s following removal of Zn^{2+}, or in cells that were not treated with Zn^{2+} at all (white bar). ($n = 10$, ANOVA, $^{****}p \leq 0.0001$). (D) Cortical neurons infected with AAV2 hSyn shZnT1 or control RFP tagged virus in addition to GCaMP6 as in A. Representative GCaMP6 fluorescence from shZnT1 or control neurons perfused with 1.8 mM Ca^{2+}-containing solution, and transiently treated with 200 μM Zn^{2+}, as in A. Right panel shows averaged rates of GCaMP6 fluorescence increases following removal of Zn^{2+} (obtained during initial 60 s following removal of Zn^{2+} ($n = 20$, t-test, $^{**}p = 0.008$).

the Ca^{2+} signal, serving as an important positive control (Fig. 5). To exclude a role for LTCC in this Ca^{2+} influx, we repeated the experiment in the presence of nifedipine (1 μM). As shown in Fig. 5C, the rate of Ca^{2+} rise upon Zn^{2+} efflux was similar in control cells and cells treated with nifedipine. This is in agreement with our previous results (Fig. 4B), showing that in this paradigm LTCC are not involved in Zn^{2+} transport. Finally, we asked if the Ca^{2+} rise is induced by ZnT1-dependent exchange of intracellular Zn^{2+} with extracellular Ca^{2+}. For this purpose, neurons were initially loaded with Zn^{2+}, and then washed with a Ca^{2+}-free solution during the Zn^{2+} efflux phase. We observed that the GCaMP6 fluorescence rise was completely abolished in the absence of extracellular Ca^{2+} (Fig. 5C), indicating that Ca^{2+} influx is coupled to, and required for Zn^{2+} efflux.

To determine whether ZnT1 is essential for the Ca^{2+} influx, we compared the rates of Ca^{2+} influx in control versus shZnT1 cells. Neurons previously co-infected with GCaMP6 and shZnT1-expressing vectors, or with GCaMP6 and RFP-only vectors, were exposed to 200 μM Zn^{2+} followed by treatment with extracellular Zn^{2+}-free solutions that contained physiological Ca^{2+} (1.8 mM). Pronounced Ca^{2+} signals were observed upon Zn^{2+} removal in control neurons but not in shZnT1 neurons (Fig. 5D), supporting an essential role for ZnT1 in mediating Ca^{2+} influx upon Zn^{2+} removal. Our results thus strongly suggest that ZnT1 represents a previously unrecognized Zn^{2+}/Ca^{2+} exchanger in neuronal plasma membranes.

Discussion

Results presented here, using Zn^{2+} and Ca^{2+} fluorescence imaging and ZnT1 knockdown, have identified ZnT1 as a previously unrecognized Zn^{2+}/Ca^{2+} exchanger. We show that ZnT1-mediated Zn^{2+} efflux occurs in the presence of extracellular Zn^{2+} at concentrations that are 4 orders of magnitude higher than its cytoplasmic levels [51, 52]. Removal of cytoplasmic Zn^{2+} against this large gradient requires a strong driving force, which can be facilitated by the similarly steep Ca^{2+} inward gradients across the plasma membrane [45]. Our data show that an inward Ca^{2+} gradient is essential for Zn^{2+} removal, and that reciprocal Zn^{2+}/Ca^{2+} transport is mediated by ZnT1. Importantly, knockdown of ZnT1 abolished both, Zn^{2+} efflux and the reciprocal Ca^{2+} influx. Both Ca^{2+} and Zn^{2+} are key elements in neuronal signaling, modulating synaptic plasticity and neuronal viability in a variety of physiological and pathophysiological conditions [1, 3, 53]. The interaction between these signaling ions is well-established, as Zn^{2+} is a strong modulator of several Ca^{2+} ionotropic pathways [2, 12, 16, 54]. Intracellular Zn^{2+} can also activate neuronal ryanodine receptors on the endoplasmic reticulum to trigger cytosolic Ca^{2+} transients [55, 56]. Moreover, Zn^{2+} is the ligand of the G protein-coupled receptor mZnR/GPR39, triggering intracellular Ca^{2+} signaling in neurons [15, 57–59]. Our results identify ZnT1 as an additional, critical regulator of signaling pathways triggered by both Zn^{2+} and Ca^{2+}.

ZnT1 function had been primarily associated with reduction in Zn^{2+} neurotoxicity [21, 60–62] under neuropathological conditions of prolonged exposure to Zn^{2+} [1, 63–65]. Neuronal Zn^{2+} permeation can occur via ZIP transporters, transient receptor potential channels (TRP), ligand and voltage gated channels [66–68]. Here, we show that ZnT1-dependent Zn^{2+}/Ca^{2+} exchange is a major pathway for neuronal Zn^{2+} efflux, modulating the initial rate of cytoplasmic Zn^{2+} rise during transient exposure to this ion, a condition that may occur following synaptic release of Zn^{2+} from ZnT3-containing terminals [12, 69, 70]. Notably, our study uses a relatively short exposure to Zn^{2+} that may more closely reflect a physiologically-relevant scenario, especially when compared to conditions previously employed to study ZnT1 activity [24]. While this is still a prolonged exposure compared to synaptic release, our data clearly shows that ZnT1-dependent efflux occurs even during the very initial loading phase and therefore suggests that it is likely physiologically relevant. Cytoplasmic Zn^{2+} modulates numerous intracellular cellular targets, including numerous kinases as well as transcription factors such as MTF-1 [71–73], ZnT1 may thus participate as an important regulatory component of these signaling cascades.

Our results also suggest that ZnT1 may be a potential trigger for specific Ca^{2+} signaling processes in neurons. While formation of ZnT1-dependent extracellular Zn^{2+} microdomains appears to be critical for the inhibition of the highly Zn^{2+}-sensitive GluN2A-containing NMDA receptors following synaptic Zn^{2+} release [17], the reciprocal cytoplasmic Ca^{2+} microdomains that are likely induced via the ZnT1-dependent Zn^{2+}/Ca^{2+} exchange could also strongly regulate NMDA receptor activity and neuronal Ca^{2+} signaling [74–76]. Importantly, Ca^{2+} entry through NMDA receptors during neuronal activity initiates gene expression and synaptic plasticity via recruitment of the Ca^{2+} binding protein calmodulin [77]. Thus, ZnT1-dependent changes in intracellular Ca^{2+} levels in proximity to the NMDA receptor could also directly affect synaptic plasticity.

During excitotoxic activity, prolonged rises in intracellular Zn^{2+} may be neurotoxic [28, 78]. The exposure to 200 μM Zn^{2+} used in some of our experiments may reflect these conditions, suggesting that ZnT1 will provide an essential neuroprotective role during pathologic conditions, as previously suggested [21, 62]. Intriguingly, as neuronal Ca^{2+} overload can, in and of itself, be toxic [79, 80], it remains to be determined whether ZnT1-dependent intracellular Ca^{2+} changes may contribute to the well-known toxic consequences of Zn^{2+} exposure in neurons [1, 2, 66, 78, 80]. Rises in intracellular Zn^{2+} induce mitochondrial dysfunction and subsequent neuronal Ca^{2+} deregulation, and thus Zn^{2+} itself is a possible component of Ca^{2+}-mediated neurotoxic signaling processes [63, 81]. It would be interesting if ZnT1, in its role as a Zn^{2+}/Ca^{2+} exchanger, may induce Ca^{2+} influx and act as an additional component of neuronal toxicity under certain circumstances. However, slow rates of ZnT1-dependent transport activity, and its attenuation of toxic NMDA-dependent Ca^{2+} influx [65], may in fact reduce, rather than enhance, excitotoxic injury. Regardless, our results highlight the intricate relationships that exist between Zn^{2+} and Ca^{2+} in neuronal signaling pathways.

Members of ZnT family that are expressed on acidic vesicles, such as ZnT5 or ZnT8, act as Zn^{2+}/H^{+} exchangers and their activity is powered by the large pH gradients across the vesicular membrane [29, 31, 32]. In contrast, ZnT1 is expressed on the plasma membrane where H^{+} gradients may not be prominent under physiological conditions, and as such would not be expected to provide the driving force for Zn^{2+} efflux. We found that lowering the extracellular pH to 6 abolished neuronal Zn^{2+} removal, suggesting that even extracellular acidic milieu does not provide a driving force that is sufficient to induce for Zn^{2+} efflux. As such, ZnT1-dependent Zn^{2+} transport is most likely not coupled to H^{+} gradients. Moreover, in the presence of acidic extracellular solutions we observed cytoplasmic acidification and further Zn^{2+} accumulation. One would expect that silencing of ZnT1, which attenuates Zn^{2+} efflux, would enhance Zn^{2+} accumulation under acidic conditions. However, our results show similar rates of Zn^{2+} accumulation upon acidification in control and shZnT1 silenced neurons. One potential explanation for this observation is that the ensuing cytoplasmic acidic conditions interfere with Zn^{2+} coordination at the His-binding sites on ZnT1, thereby inhibiting ZnT1-dependent Zn^{2+} efflux in control neurons, resulting in similar Zn^{2+} accumulation rates as in ZnT1 silenced neurons. Indeed, ZnT8-dependent Zn^{2+} transport into acidic organelles depends on release of Zn^{2+} from His-residues in the lumen acidic conditions [31]. Another scenario is that the cellular acidification, following exposure of neurons to pH 6, results in rapid liberation of Zn^{2+} from metal binding proteins or other cytosolic ligands [40, 82], which cannot be effectively counteracted by ZnT1-mediated transport. A recent study, using reconstituted liposomes expressing ZnT1 and the E. coli F0F1 ATP synthase, demonstrated ZnT1-dependent H^{+} transport in the presence mM concentrations of Zn^{2+} and a steep ATP-dependent outward H^{+} gradient [83]. However, it is unclear if the H^{+} transport was coupled to ZnT1-dependent transport as ZnT1-lacking reconstituted vesicles also effectively transported H^{+}, and direct measurement of Zn^{2+} transport

was not demonstrated. Moreover, kinetic properties of ZnT1 obtained in this study, using 1–10 mM Zn^{2+}, are dramatically different than those obtained for other ZnT members in the same preparation [84]. Although we cannot rule out a possible effect of acidic intracellular pH on the Zn^{2+} binding site of ZnT1, our results, strongly indicate that ZnT1 provides limited or no Zn^{2+}/H^{+} exchange across neuronal cell membranes. Another putative counter ion to Zn^{2+} is Na^{+}, which is present at a very high inward gradient supporting numerous transporters [41, 85], and could also support Zn^{2+} efflux. However, previous studies addressing the mechanism underlying transport by ZnTs indicated that Na^{+} is not transported by these proteins [29, 86]. The observed dramatic modulation of transport by Ca^{2+} suggests that ZnT1 is a Zn^{2+}/Ca^{2+} exchanger.

The Zn^{2+} metal-binding site, conserved among most members of the ZnT family is composed of a His-Asp-His-Asp-motif [6, 87]. Analysis of the coordination geometries of metal ions indicates that Zn^{2+}, among other metals, has a preference to His-residues within the tetrahedral geometry of this binding site [87]. Indeed, replacement of a single His-residue to an Asp-within the Zn^{2+} binding site in vesicular ZnT5 or ZnT8 abolishes their binding selectivity between Zn^{2+} and Cd^{2+} [30]. Bioinformatics scanning of residues that are located on Ca^{2+}-binding sites of proteins, identified Asp-residues as having the highest affinity for Ca^{2+} [86]. The ZnT1 putative binding site that is formed of a His-Asp-His-Asp-motif is therefore composed of residues that have the highest affinity for both Zn^{2+} (His) and Ca^{2+} (Asp). However, Ca^{2+} binding sites have a distinct conformation with several Asp-residues that are not shared with the Zn^{2+} binding site on ZnT1. Such distinct binding sites are also described for other proteins that bind both Zn^{2+} and Ca^{2+} [88–90]. While the His-Asp-His-Asp-motif in the metal binding site of ZnT1 is preserved among most members of the SLC30A family, there is substitution of Asn-for His-at the metal binding site of ZnT10 (SLC30A10), which protects neurons from manganese toxicity [91]. Interestingly, Zn^{2+} has very low preference to Asn, and, indeed, ZnT10 is indifferent to this metal ion [86]. Both Ca^{2+} and Mn^{2+} show preference to Asn-binding, leading ZnT10 to function as a Mn^{2+}/Ca^{2+} exchanger [86]. It remains to be determined whether other ZnT family members that have the His-Asp-His-Asp-motif are capable of mediating Zn^{2+}/Ca^{2+} exchange when exposed to varying Ca^{2+} gradients.

Our study identifies ZnT1 as a physiologically relevant modulator of neuronal Zn^{2+} and Ca^{2+} transport in neurons, and, as such, may strongly influence synaptic signaling and plasticity.

Materials and methods

All experimental procedures performed on animals are done in accordance with a protocol approved by the committee for Ethical Care and Use of Animals in Research at the Faculty of Health Sciences at Ben-Gurion University of the Negev.

Primary cortical neurons. Primary cortical neurons were obtained from newborn RccB57 (WT) mice (P1–2). Cortices were dissociated with mechanic pipetting in Hanks' balanced salts solution (HBSS) (4 ml HBSS and 20 mM HEPES pH 7.4). The cell suspension was cultured in neurobasal growth medium, supplemented with 5% fetal bovine serum (FBS), 2% B-27, 1% Glutamax-100X, and 1 μg/ml gentamicin. After 24 h growth medium was changed to neurobasal growth medium, supplemented with 2% B-27 and 1% Glutamax-100X. All cells were cultured in a humidified atmosphere of 5% CO_2 at 37 °C. For imaging experiments, 15×10^4 cells were seeded per 50 μg poly-D-lysin-treated coverslips (12 mm) in 24 well plates.

Fluorescent Imaging. The imaging system consists of an Olympus inverted microscope, and a CoolLED charge coupled device. Fluorescent imaging measurements are acquired with Cell Sense (Olympus micro Imaging software). Zinc imaging is conducted as follows: First, cells are seeded on coverslips and grow for two weeks. Then, cells are loaded with dyes according to the experiment and perfused with Ringer's solution (composed of, in mM: 120 NaCl; 5.4 KCl; 1.8 CaCl2; 0.8 MgCl2; 10 HEPES; 10 glucose; pH 7.4/ pH 6/ pH 8). Coverslips are then mounted in a microscope chamber that allows rapid solution exchange. For zinc imaging FluoZin-3 (1.5 μM), a Zn^{2+}-selective indicator was used [36]. Staining performed for 25 min and subsequently washed for at least 15 min. FluoZin-3 is excited at ~494 nm and imaged with a ~516 nm long-pass filter. For pH changes, staining was performed using BCECF (2′,7′-Bis-(2-Carboxyethyl)−5-(and-6)-Carboxyfluorescein) dye for 20 min and washed for 10 min. BCECF is a radiometric dye excited at ~490 nm versus its isobestic point of ~440 nm and is detected at 535 nm [58]. For calcium measurements we used the GCaMP6 slow indicator. Neurons (DIV 7,8) were infected with hSyn AAV2 GCaMP6 virus, and used for imaging 7 days following infection. GCaMP6 is excited at ~494 nm and imaged with a ~516 nm long-pass filter. Rates of fluorescence change were calculated by linear fit to the initial phase of the response and were averaged and presented in bar graphs. All results shown are average ±SD, presented as boxplots, of at least three independent experiments.

Real time-PCR analysis. RT-PCR was used to determine ZnT1 mRNA levels in cortical cultures infected with AAV2 hSyn shZnT1 virus versus control RFP tagged vector (Fig. 1), or in neurons pre-treated with Zn^{2+} versus control neurons that were exposed to a similar medium replacement without Zn^{2+} (Fig. 2). RNA was purified with PureLink RNA Mini Kit (Ambion, ThermoFisher Scientific) as described by the manufacturer and treated with DNase (Invitrogen) in the process. One μg RNA was converted to cDNA using Quanta cDNA synthesis Kit as described by the manufacturer. cDNA was diluted 1:5 with ultrapure water and subjected to real time PCR procedure (Taqman). Primers and probes were supplied by Integrated DNA Technologies. Gene expression levels were normalized to Actin. The following primers were used: ZnT1-Mm.PT.58.42957893; β Actin - Mm.PT.58.33257376.gs

Generation of AAV2–323 vector and gene silencing. Viral vectors based on adeno-associated virus (AAV) for expression of short hairpin RNA (shRNA) were utilized for targeted silencing of ZnT1 transporter in cortical neuronal cultures. shRNA sequences for ZnT1 as well as control were supplied by TransOMIC Technologies, USA (shZnT1 – sense 5′-AAAGGCGCCAAC AGTTAGCATA-3′, all shRNAs contained TAGT-GAAGCCACAGA TGTA mir-30a loop). All the shRNA sequences were preceded by the RFP gene under the Human synapsin 1 gene promoter. Control vector contained the RFP sequence alone, since scrambled controls resulted in unexplained massive neuronal death. Only RFP-positive cells were utilized for any experimental procedures involving the AAV targeted silencing. AAV2–323 was produced as described previously [92]. Briefly, AAVs were generated in HEK-293T cells (ATCC) using calcium phosphate transfection. To obtain the packed virions, 72 h after the transfection cells were lysed in lysis buffer (150 mM NaCl and 500 mM Tris) by 3 freeze-thaw cycles (on 37 °C and −80 °C) after which the buffer was incubated with 100 U/mL benzonase (Sigma; E1014) for 1 h on 37 °C. The lysate was stored on 4 °C until used.

Immunocytochemistry. For immunocytochemistry analysis, 14–16DIV neurons seeded on coverslips were washed and embedded with 4% PFA. Sections were exposed to 0.3% triton solution as antigen retrieval step. Blocking was done using blocking buffer (5% milk, 0.1% triton) for 1 h at room temperature. Then, cells were incubated with primary antibodies (see below) diluted in 1:2 dilution of blocking solution for 1 h. The next day, sections were washed and incubated in fluorophore conjugated secondary antibodies for 1 h in the dark. Primary antibodies used: Anti-ZnT1 (SLC30A1) Antibody (Alomone #AZT-011) 1:200, Anti Tau (SySy #314 004) 1:500, Anti MAP 2 (SySy #188 011) 1:300, Anti GluN2A/NR2A (NeuroMab #75–288) 1:300. secondary antibodies used: Alexa488 donkey anti mouse, Alexa488 or Alexa647 conjugated goat anti rabbit, Alexa594 conjugated goat anti guinea pig, Jackson ImmunoResearch Laboratories. Finally, sections were washed and mounted using Dapi-containing immunomount to mark nuclei.

Western-blot analysis. Protein expression was monitored using western blot analysis. Cortical cultured neurons were tested for ZnT1 protein levels after infection with shZnT1 viral vector (Fig.1) or after

treatment with Zn^{2+} (50 μM Zn^{2+} for 12 h, Fig. 2). Neuronal cultures were infected on DIV7–8 and cells were harvest a week later into lysis buffer (50 mM HEPES pH 7.4, 10% glycerol, 10 mM $MgCl_2$, 150 mM NaCl, 1 mM EDTA, 1 mM EGTA, 1% (v/v) Triton X-100) in the presence of Protease Inhibitor Cocktail (1:50 complete, Sigma-Aldrich, Israel). Lysates were placed on ice for 10 min and centrifuged for 30 min (12,000 rpm) at 4 °C. Supernatants were collected and protein concentrations were determined using Bio-Rad protein assay, SDS sample buffer was added, and samples were boiled for 5 min and then frozen at −20 °C until used. Proteins were separated on an SDS-PAGE and analyzed using antibodies raised against mZnT1 (SYSY #166–103, or Alomone #AZT-011) and mActin (1:10,000, MP-Biomedicals) at 4 °C overnight. The next day membranes were exposed to goat anti-mouse or anti-rabbit horseradish peroxidase-conjugated antibodies (Jackson ImmunoResearch Laboratories) for 1 h in RT. Densitometry analysis of expression level was performed using EZQuant-Gel software (EZQuant, Israel). Protein levels were estimated as the ratio of ZnT1 to Actin in each sample. Each bar graph represents an average of at least three independent experiments.

Cellular viability detection. Cortical neurons were treated with 50 μM Zn^{2+} for 12 h in MEM medium supplemented with 0.01% BSA and 25 mM HEPES. Growth medium was collected and LDH release was determined using a commercial kit (ab102526, Abcam, Inc).

Statistical analysis. Each boxplot represents data from n repetitions that denotes the number of coverslips analyzed for each condition (for imaging paradigms or immunofluorescence analysis) with about 20 neurons monitored in each coverslip. For mRNA or protein quantification, n denotes the number of lysates used. All experiments were performed on at least three independent cortical culture preparations. Statistical analysis was performed using Student's *t*-test with no assume equal SDs, or ANOVA using Tukey multiple correction test, where appropriate. *$p < 0.05$, **$p < 0.01$, ***$p < 0.001$, ****$p \leq 0.0001$, ns-non-significant.

CRediT authorship contribution statement

Noa Gottesman: Investigation, Formal analysis, Writing – original draft, Visualization, Writing – review & editing. **Hila Asraf:** Investigation, Methodology, Validation, Writing – review & editing. **Milos Bogdanovic:** Investigation, Validation. **Isr Sekler:** Methodology, Writing – review & editing. **Thanos Tzounopoulos:** Conceptualization, Writing – review & editing. **Eli Aizenman:** Conceptualization, Methodology, Writing – review & editing. **Mic Hershfinkel:** Conceptualization, Methodology, Formal analysis, Writing – original draft, Writing – review & editing, Supervision, Funding acquisition.

Declaration of Competing Interest

Authors declare no competing interests.

Acknowledgments

This work was funded by the National Science Foundation-US-Israel Binational Science foundation grant NSF-IOS-BSF 1655480, jointly awarded to MH, TT and EA. MH is also funded by Israel Science Foundation Grant 812/20.

Supplementary materials

Supplementary data associated with this article can be found, in the online version, at 10.1016/j.ejor.2015.01.016.

References

[1] S.L. Sensi, P. Paoletti, J.Y. Koh, E. Aizenman, A.I. Bush, M. Hershfinkel, The neurophysiology and pathology of brain zinc, J. Neurosci. 31 (2011) 16076–16085.
[2] R.F. Krall, T. Tzounopoulos, E. Aizenman, The function and regulation of zinc in the brain, Neuroscience 15 (2021) 00017–00018.
[3] H.Y. Liu, J.R. Gale, I.J. Reynolds, J.H. Weiss, E. Aizenman, The multifaceted roles of zinc in neuronal mitochondrial dysfunction, Biomedicines 9 (2021).
[4] N. Levaot, M. Hershfinkel, How cellular Zn(2 +) signaling drives physiological functions, Cell Calcium 75 (2018) 53–63.
[5] T.E. Thingholm, L. Rönnstrand, P.A. Rosenberg, Why and how to investigate the role of protein phosphorylation in ZIP and ZnT zinc transporter activity and regulation, Cell Mol. Life Sci. 77 (2020) 3085–3102.
[6] T. Kambe, K.M. Taylor, D. Fu, Zinc transporters and their functional integration in mammalian cells, J. Biol. Chem. 296 (2021), 100320.
[7] B.B. McAllister, R.H. Dyck, Zinc transporter 3 (ZnT3) and vesicular zinc in central nervous system function, Neurosci. Biobehav. Rev. 80 (2017) 329–350.
[8] R.D. Palmiter, T.B. Cole, C.J. Quaife, S.D. Findley, ZnT-3, a putative transporter of zinc into synaptic vesicles, Proc. Natl. Acad. Sci. U. S. A. 93 (1996) 14934–14939.
[9] S. Kouvaros, M. Kumar, T. Tzounopoulos, Synaptic zinc enhances inhibition mediated by somatostatin, but not parvalbumin, cells in mouse auditory cortex, Cereb Cortex 30 (2020) 3895–3909.
[10] A.M. Vergnano, N. Rebola, L.P. Savtchenko, P.S. Pinheiro, M. Casado, B.L. Kieffer, D.A. Rusakov, C. Mulle, P. Paoletti, Zinc dynamics and action at excitatory synapses, Neuron 82 (2014) 1101–1114.
[11] P. Paoletti, P. Ascher, J. Neyton, High-affinity zinc inhibition of NMDA NR1-NR2A receptors, J. Neurosci. 17 (1997) 5711–5725.
[12] B.I. Kalappa, C.T. Anderson, J.M. Goldberg, S.J. Lippard, T. Tzounopoulos, AMPA receptor inhibition by synaptically released zinc, Proc. Natl. Acad. Sci. U. S. A. 112 (2015) 15749–15754.
[13] B.Y. Choi, D.K. Hong, J.H. Jeong, B.E. Lee, J.Y. Koh, S.W. Suh, Zinc transporter 3 modulates cell proliferation and neuronal differentiation in the adult hippocampus, Stem. Cells 38 (2020) 994–1006.
[14] B.B. McAllister, A. Pochakom, S. Fu, R.H. Dyck, Effects of social defeat stress and fluoxetine treatment on neurogenesis and behavior in mice that lack zinc transporter 3 (ZnT3) and vesicular zinc, Hippocampus 30 (2020) 623–637.
[15] L. Besser, E. Chorin, I. Sekler, W.F. Silverman, S. Atkin, J.T. Russell, M. Hershfinkel, Synaptically released zinc triggers metabotropic signaling via a zinc-sensing receptor in the hippocampus, J. Neurosci. 29 (2009) 2890–2901.
[16] C.T. Anderson, R.J. Radford, M.L. Zastrow, D.Y. Zhang, U.P. Apfel, S.J. Lippard, T. Tzounopoulos, Modulation of extrasynaptic NMDA receptors by synaptic and tonic zinc, Proc. Natl. Acad. Sci. U. S. A. 112 (2015) E2705–E2714.
[17] R.F. Krall, A. Moutal, M.B. Phillips, H. Asraf, J.W. Johnson, R. Khanna, [illegible] T. Tzounopoulos, Synaptic zinc inhibition of NMDA receptors depends on the association of GluN2A with the zinc transporter ZnT1, Sci. Adv. 6 (2020).
[18] [illegible] J. Wang, S.K. Dey, R.D. Palmiter, Mouse zinc transporter 1 gene encodes an essential function during early embryonic development, Genesis 40 (2004) 74–81.
[19] R.D. Palmiter, S.D. Findley, Cloning and functional characterization of a mammalian zinc transporter that confers resistance to zinc, Embo. J. 14 (1995) 639–649.
[20] Y.B. Nitzan, I. Sekler, M. Hershfinkel, A. Moran, W.F. Silverman, Postnatal regulation of ZnT-1 expression in the mouse brain, Brain Res. Dev. Brain Res. 137 (2002) 149–157.
[21] E. Ohana, I. Sekler, T. Kaisman, N. Kahn, J. Cove, W.F. Silverman, A. Amsterdam, M. Hershfinkel, Silencing of ZnT-1 expression enhances heavy metal influx and toxicity, J. Mol. Med. 84 (2006) 753–763 (Berl).
[22] I. Sekler, A. Moran, M. Hershfinkel, A. Dori, A. Margulis, N. Birenzweig, Y. Nitzan, W.F. Silverman, Distribution of the zinc transporter ZnT-1 in comparison with chelatable zinc in the mouse brain, J. Comp. Neurol. 447 (2002) 201–209.
[23] C. Sindreu, Á. Bayés, X. Altafaj, J. Pérez-Clausell, Zinc transporter-1 concentrates at the postsynaptic density of hippocampal synapses, Mol. Brain 7 (2014) 16.
[24] Y. Qin, D. Thomas, C.P. Fontaine, R.A. Colvin, Silencing of ZnT1 reduces Zn2 + efflux in cultured cortical neurons, Neurosci. Lett. 450 (2009) 206–210.
[25] Y. Nishito, T. Kambe, Zinc transporter 1 (ZNT1) expression on the cell surface is elaborately controlled by cellular zinc levels, J. Biol. Chem. 294 (2019) 15686–15697.
[26] S.J. Langmade, R. Ravindra, P.J. Daniels, G.K. Andrews, The transcription factor MTF-1 mediates metal regulation of the mouse ZnT1 gene, J. Biol. Chem. 275 (2000) 34803–34809.
[27] C. Nolte, A. Gore, I. Sekler, W. Kresse, M. Hershfinkel, A. Hoffmann, H. Kettenmann, A. Moran, ZnT-1 expression in astroglial cells protects against zinc toxicity and slows the accumulation of intracellular zinc, Glia 48 (2004) 145–155.
[28] Y.V. Medvedeva, B. Lin, C.W. Shuttleworth, J.H. Weiss, Intracellular Zn2 + accumulation contributes to synaptic failure, mitochondrial depolarization, and cell death in an acute slice oxygen-glucose deprivation model of ischemia, J. Neurosci. 29 (2009) 1105–1114.
[29] E. Ohana, E. Hoch, C. Keasar, T. Kambe, O. Yifrach, M. Hershfinkel, I. Sekler, Identification of the Zn2 + binding site and mode of operation of a mammalian Zn2 + transporter, J. Biol. Chem. 284 (2009) 17677–17686.
[30] E. Hoch, W. Lin, J. Chai, M. Hershfinkel, D. Fu, I. Sekler, Histidine pairing at the metal transport site of mammalian ZnT transporters controls Zn2 + over Cd2+ selectivity, Proc. Natl. Acad. Sci. U. S. A. 109 (2012) 7202–7207.

[31] J. Xue, T. Xie, W. Zeng, Y. Jiang, X.C. Bai, Cryo-EM structures of human ZnT8 in both outward- and inward-facing conformations, Elife 9 (2020) 58823.
[32] M. Lu, J. Chai, D. Fu, Structural basis for autoregulation of the zinc transporter YiiP, Nat. Struct. Mol. Biol. 16 (2009) 1063–1067.
[33] R.P. Kraig, C.R. Ferreira-Filho, C. Nicholson, Alkaline and acid transients in cerebellar microenvironment, J. Neurophysiol. 49 (1983) 831–850.
[34] M. Chesler, K. Kaila, Modulation of pH by neuronal activity, Trends Neurosci. 15 (1992) 396–402.
[35] M. Mellone, S. Pelucchi, L. Alberti, A.A. Genazzani, M. Di Luca, F. Gardoni, Zinc transporter-1: a novel NMDA receptor-binding protein at the postsynaptic density, J. Neurochem. 132 (2015) 159–168.
[36] M.J. Devinney, I.J. Reynolds, K.E. Dineley, Simultaneous detection of intracellular free calcium and zinc using fura-2FF and FluoZin-3, Cell Calcium 37 (2005) 225–232.
[37] K.E. Dineley, L.M. Malaiyandi, I.J. Reynolds, A reevaluation of neuronal zinc measurements: artifacts associated with high intracellular dye concentration, Mol. Pharmacol. 62 (2002) 618–627.
[38] J.Y. Koh, D.W. Choi, Quantitative determination of glutamate mediated cortical neuronal injury in cell culture by lactate dehydrogenase efflux assay, J. Neurosci. Methods 20 (1987) 83–90.
[39] Y. Golan, R. Alhadeff, A. Warshel, Y.G. Assaraf, ZnT2 is an electroneutral proton-coupled vesicular antiporter displaying an apparent stoichiometry of two protons per zinc ion, PLoS Comput. Biol. 15 (2019), e1006882.
[40] L. Kiedrowski, Cytosolic acidification and intracellular zinc release in hippocampal neurons, J. Neurochem. 121 (2012) 438–450.
[41] J. Orlowski, S. Grinstein, Diversity of the mammalian sodium/proton exchanger SLC9 gene family, Pflugers. Arch. 447 (2004) 549–565.
[42] G.N. Rao, C. Sardet, J. Pouysségur, B.C. Berk, Phosphorylation of Na(+)-H+ antiporter is not stimulated by phorbol ester and acidification in granulocytic HL-60 cells, Am. J. Physiol. 264 (1993) C1278–C1284.
[43] R.A. Colvin, N. Davis, R.W. Nipper, P.A. Carter, Evidence for a zinc/proton antiporter in rat brain, Neurochem. Int. 36 (2000) 539–547.
[44] R.A. Colvin, pH dependence and compartmentalization of zinc transported across plasma membrane of rat cortical neurons, Am. J. Physiol. Cell Physiol. 282 (2002) C317–C329.
[45] M. Brini, T. Calì, D. Ottolini, E. Carafoli, Neuronal calcium signaling: function and dysfunction, Cell Mol. Life Sci. 71 (2014) 2787–2814.
[46] S.L. Sensi, H.Z. Yin, S.G. Carriedo, S.S. Rao, J.H. Weiss, Preferential Zn^{2+} influx through Ca^{2+}-permeable AMPA/kainate channels triggers prolonged mitochondrial superoxide production, Proc. Natl. Acad. Sci. U. S. A. 96 (1999) 2414–2419.
[47] T. Priel, M. Hershfinkel, Zinc influx and physiological consequences in the beta-insulinoma cell line, Min6, Biochem. Biophys. Res. Commun. 346 (2006) 205–212.
[48] S. Yamasaki, A. Hasegawa, S. Hojyo, W. Ohashi, T. Fukada, K. Nishida, T. Hirano, A novel role of the L-type calcium channel α1D subunit as a gatekeeper for intracellular zinc signaling: zinc wave, PLoS ONE 7 (2012) e39654.
[49] E.P.S. Pratt, L.J. Damon, K.J. Anson, A.E. Palmer, Tools and techniques for illuminating the cell biology of zinc, Biochim. Biophys. Acta Mol. Cell Res. 1868 (2021), 118865.
[50] A.I. Kostyuk, A.D. Demidovich, D.A. Kotova, V.V. Belousov, D.S. Bilan, Circularly Permuted Fluorescent Protein-Based Indicators: history, principles, and classification, Int. J. Mol. Sci. 20 (2019).
[51] C.J. Frederickson, L.J. Giblin, A. Krezel, D.J. McAdoo, R.N. Mueller, Y. Zeng, R. V. Balaji, R. Masalha, R.B. Thompson, C.A. Fierke, J.M. Sarvey, M. de Valdenebro, D.S. Prough, M.H. Zornow, Concentrations of extracellular free zinc (pZn)e in the central nervous system during simple anesthetization, ischemia and reperfusion, Exp. Neurol. 198 (2006) 285–293.
[52] S.L. Sensi, P. Paoletti, A.I. Bush, I. Sekler, Zinc in the physiology and pathology of the CNS, Nat. Rev. Neurosci. 10 (2009) 780–791.
[53] A. Granzotto, S.L. Sensi, Intracellular zinc is a critical intermediate in the excitotoxic cascade, Neurobiol. Dis. 81 (2015) 25–37.
[54] J. Rachline, F. Perin-Dureau, A.Le Goff, J. Neyton, P. Paoletti, The micromolar zinc-binding domain on the NMDA receptor subunit NR2B, J. Neurosci. 25 (2005) 308–317.
[55] A.J. Schulien, J.A. Justice, R. Di Maio, Z.P. Wills, N.H. Shah, E. Aizenman, Zn(2+) -induced Ca(2+) release via ryanodine receptors triggers calcineurin-dependent redistribution of cortical neuronal Kv2.1 K(+) channels, J. Physiol. 594 (2016) 2647–2659.
[56] J. Woodier, R.D. Rainbow, A.J. Stewart, S.J. Pitt, Intracellular zinc modulates cardiac ryanodine receptor-mediated calcium release, J. Biol. Chem. 290 (2015) 17599–17610.
[57] E. Chorin, O. Vinograd, I. Fleidervish, D. Gilad, S. Herrmann, I. Sekler, E. Aizenman, M. Hershfinkel, Upregulation of KCC2 activity by zinc-mediated neurotransmission via the mZnR/GPR39 receptor, J. Neurosci. 31 (2011) 12916–12926.
[58] R.A. Saadi, K. He, K.A. Hartnett, K. Kandler, M. Hershfinkel, E. Aizenman, SNARE-dependent upregulation of potassium chloride co-transporter 2 activity after metabotropic zinc receptor activation in rat cortical neurons in vitro, Neuroscience 210 (2012) 38–46.
[59] D. Gilad, S. Shorer, M. Ketzef, A. Friedman, I. Sekler, E. Aizenman, M. Hershfinkel, Homeostatic regulation of KCC2 activity by the zinc receptor mZnR/GPR39 during seizures, Neurobiol. Dis. 81 (2015) 4–13.
[60] A. Granzotto, L.M.T. Canzoniero, S.L. Sensi, A neurotoxic ménage-à-trois: glutamate, calcium, and zinc in the excitotoxic cascade, Front. Mol. Neurosci. 13 (2020), 600089.
[61] M. Tsuda, K. Imaizumi, T. Katayama, K. Kitagawa, A. Wanaka, M. Tohyama, T. Takagi, Expression of zinc transporter gene, ZnT-1, is induced after transient forebrain ischemia in the gerbil, J. Neurosci. 17 (1997) 6678–6684.
[62] R.D. Palmiter, Protection against zinc toxicity by metallothionein and zinc transporter 1, Proc. Natl. Acad. Sci. U. S. A. 101 (2004) 4918–4923.
[63] T.A. Vander Jagt, J.A. Connor, J.H. Weiss, C.W. Shuttleworth, Intracellular Zn2 + increases contribute to the progression of excitotoxic Ca2 + increases in apical dendrites of CA1 pyramidal neurons, Neuroscience 159 (2009) 104–114.
[64] M.A. Aras, E. Aizenman, Redox regulation of intracellular zinc: molecular signaling in the life and death of neurons, Antioxid Redox Signal 15 (2011) 2249–2263.
[65] E. Aizenman, R.H. Loring, I.J. Reynolds, P.A. Rosenberg, The redox biology of excitotoxic processes: the NMDA receptor, topa quinone, and the oxidative liberation of intracellular zinc, Front. Neurosci. 14 (2020) 778.
[66] S.L. Sensi, L.M. Canzoniero, S.P. Yu, H.S. Ying, J.Y. Koh, G.A. Kerchner, D.W. Choi, Measurement of intracellular free zinc in living cortical neurons: routes of entry, J. Neurosci. 17 (1997) 9554–9564.
[67] J. Gibon, P. Tu, S. Bohic, P. Richaud, J. Arnaud, M. Zhu, G. Boulay, A. Bouron, The over-expression of TRPC6 channels in HEK-293 cells favours the intracellular accumulation of zinc, Biochim. Biophys. Acta 1808 (2011) 2807–2818.
[68] S.E. Park, J.H. Song, C. Hong, D.E. Kim, J.W. Sul, T.Y. Kim, B.R. Seo, I. So, S. Y. Kim, D.J. Bae, M.H. Park, H.M. Lim, I.J. Baek, A. Riccio, J.Y. Lee, W.H. Shim, B. Park, J.Y. Koh, J.J. Hwang, Contribution of zinc-dependent delayed calcium influx via TRPC5 in oxidative neuronal death and its prevention by novel TRPC antagonist, Mol. Neurobiol. 56 (2019) 2822–2835.
[69] J. Qian, J.L. Noebels, Visualization of transmitter release with zinc fluorescence detection at the mouse hippocampal mossy fibre synapse, J. Physiol. 566 (2005) 747–758.
[70] Y. Li, C.J. Hough, C.J. Frederickson, J.M. Sarvey, Induction of mossy fiber – >Ca3 long-term potentiation requires translocation of synaptically released Zn2 + , J. Neurosci. 21 (2001) 8015–8025.
[71] D. Atar, P.H. Backx, M.M. Appel, W.D. Gao, E. Marban, Excitation-transcription coupling mediated by zinc influx through voltage-dependent calcium channels, J. Biol. Chem. 270 (1995) 2473–2477.
[72] A.J. Stewart, S.J. Pitt, Zinc controls RyR2 activity during excitation-contraction coupling, Channels 9 (2015) 227–229 (Austin).
[73] W. Maret, Zinc in cellular regulation: the nature and significance of "zinc signals", Int. J. Mol. Sci. 18 (2017).
[74] G.E. Hardingham, F.J. Arnold, H. Bading, A calcium microdomain near NMDA receptors: on switch for ERK-dependent synapse-to-nucleus communication, Nat. Neurosci. 4 (2001) 565–566.
[75] I. Medina, X. Leinekugel, Y. Ben-Ari, Calcium-dependent inactivation of the monosynaptic NMDA EPSCs in rat hippocampal neurons in culture, Eur. J. Neurosci. 11 (1999) 2422–2430.
[76] C.F. Zorumski, J. Yang, G.D. Fischbach, Calcium-dependent, slow desensitization distinguishes different types of glutamate receptors, Cell Mol. Neurobiol. 9 (1989) 95–104.
[77] K. Deisseroth, P.G. Mermelstein, H. Xia, R.W. Tsien, Signaling from synapse to nucleus: the logic behind the mechanisms, Curr. Opin. Neurobiol. 13 (2003) 354–365.
[78] J.H. Weiss, D.M. Hartley, J.Y. Koh, D.W. Choi, AMPA receptor activation potentiates zinc neurotoxicity, Neuron 10 (1993) 43–49.
[79] K. Szydlowska, M. Tymianski, Calcium, ischemia and excitotoxicity, Cell Calcium 47 (2010) 122–129.
[80] C.J. Stork, Y.V. Li, Elevated cytoplasmic free zinc and increased reactive oxygen species generation in the context of brain injury, Acta Neurochir. Suppl. 121 (2016) 347–353.
[81] S.G. Ji, Y.V. Medvedeva, H.L. Wang, H.Z. Yin, J.H. Weiss, Mitochondrial Zn(2 +) accumulation: a potential trigger of hippocampal ischemic injury, Neuroscientist 25 (2019) 126–138.
[82] L. Kiedrowski, Proton-dependent zinc release from intracellular ligands, J. Neurochem. 130 (2014) 87–96.
[83] C.A. Cotrim, R.J. Jarrott, A.E. Whitten, H.G. Choudhury, D. Drew, J.L. Martin, Heterologous expression and biochemical characterization of the human zinc transporter 1 (ZnT1) and its soluble C-terminal domain, Front. Chem. 9 (2021), 667803.
[84] C. Merriman, Q. Huang, G.A. Rutter, D. Fu, Lipid-tuned zinc transport activity of human ZnT8 protein correlates with risk for type-2 diabetes, J. Biol. Chem. 291 (2016) 26950–26957.
[85] K. Jayaraman, A.K. Das, D. Luethi, D. Szöllősi, G.J. Schütz, M.E.A. Reith, H.H. Sitte, T. Stockner, SLC6 transporter oligomerization, J. Neurochem. 157 (2021) 919–929.
[86] M. Levy, N. Elkoshi, S. Barber-Zucker, E. Hoch, R. Zarivach, M. Hershfinkel, I. Sekler, Zinc transporter 10 (ZnT10)-dependent extrusion of cellular Mn(2 +) is driven by an active Ca(2 +)-coupled exchange, J. Biol. Chem. 294 (2019) 5879–5889.
[87] S. Barber-Zucker, B. Shaanan, R. Zarivach, Transition metal binding selectivity in proteins and its correlation with the phylogenomic classification of the cation diffusion facilitator protein family, Sci. Rep. 7 (2017) 16381.
[88] K. Murakami, L.J. Berliner, A distinct zinc binding site in the alpha-lactalbumins regulates calcium binding. Is there a physiological role for this control? Biochemistry 22 (1983) 3370–3374.
[89] J. Baudier, D. Gérard, Ions binding to S100 proteins: structural changes induced by calcium and zinc on S100a and S100b proteins, Biochemistry 22 (1983) 3360–3369.

[90] E. Picello, E. Damiani, A. Margreth, Low-affinity Ca(2 +)-binding sites versus Zn(2 +)-binding sites in histidine-rich Ca(2 +)-binding protein of skeletal muscle sarcoplasmic reticulum, Biochem. Biophys. Res. Commun. 186 (1992) 659–667.
[91] C.A. Taylor, S. Hutchens, C. Liu, T. Jursa, W. Shawlot, M. Aschner, D.R. Smith, S. Mukhopadhyay, SLC30A10 transporter in the digestive system regulates brain manganese under basal conditions while brain SLC30A10 protects against neurotoxicity, J. Biol. Chem. 294 (2019) 1860–1876.
[92] R.C. Challis, S. Ravindra Kumar, K.Y. Chan, C. Challis, K. Beadle, M.J. Jang, H. M. Kim, P.S. Rajendran, J.D. Tompkins, K. Shivkumar, B.E. Deverman, V. Gradinaru, Systemic AAV vectors for widespread and targeted gene delivery in rodents, Nat. Protoc. 14 (2019) 379–414.